Genetics in Medicine (2023) 25, 100922

ELSEVIER

Genetics in Medicine
An Official Journal of the ACMG

www.journals.elsevier.com/genetics-in-medicine

ARTICLE

Missense variants in *RPH3A* cause defects in excitatory synaptic function and are associated with a clinically variable neurodevelopmental disorder

ARTICLE INFO

Article history:
Received 19 October 2022
Received in revised form
22 June 2023
Accepted 25 June 2023
Available online 1 July 2023

Keywords:
Epilepsy
Excitatory synapse
Neurodevelopmental disorder
Rabphilin
RPH3A

ABSTRACT

Purpose: *RPH3A* encodes a protein involved in the stabilization of GluN2A subunit of N-methyl-D-aspartate (NMDA)-type glutamate receptors at the cell surface, forming a complex essential for synaptic plasticity and cognition. We investigated the effect of variants in *RPH3A* in patients with neurodevelopmental disorders.

Methods: By using trio-based exome sequencing, GeneMatcher, and screening of 100,000 Genomes Project data, we identified 6 heterozygous variants in *RPH3A*. In silico and in vitro models, including rat hippocampal neuronal cultures, have been used to characterize the effect of the variants.

Results: Four cases had a neurodevelopmental disorder with untreatable epileptic seizures [p.(Gln73His)*dn*; p.(Arg209Lys); p.(Thr450Ser)*dn*; p.(Gln508His)], and 2 cases [p.(Arg235Ser); p.(Asn618Ser)*dn*] showed high-functioning autism spectrum disorder. Using neuronal cultures, we demonstrated that p.(Thr450Ser) and p.(Asn618Ser) reduce the synaptic localization of GluN2A; p.(Thr450Ser) also increased the surface levels of GluN2A. Electrophysiological recordings showed increased GluN2A-dependent NMDA ionotropic glutamate receptor currents for both variants and alteration of postsynaptic calcium levels. Finally, expression of the Rph3A^{Thr450Ser} variant in neurons affected dendritic spine morphology.

Conclusion: Overall, we provide evidence that missense gain-of-function variants in *RPH3A* increase GluN2A-containing NMDA ionotropic glutamate receptors at extrasynaptic sites, altering synaptic function and leading to a clinically variable neurodevelopmental presentation ranging from untreatable epilepsy to autism spectrum disorder.

Introduction

N-methyl-D-aspartate ionotropic glutamate receptors (NMDARs) drive key cellular events involved in neuronal differentiation and synapse formation.[1] These processes are correlated to dynamic modifications of NMDAR subunit composition, including the developmental switch from GluN2B- to GluN2A-containing receptors.[2] Several pathogenic variants involving NMDAR subunits (eg, GRIN proteins) have been identified and associated with a wide spectrum of neurodevelopmental disorders (NDDs), including epilepsy and autism spectrum disorder (ASD).[3-9] Among these, pathogenic variants affecting the *GRIN2A*

Lisa Pavinato, Jennifer Stanic, Fabrizio Gardoni, and Alfredo Brusco contributed equally.
*Correspondence and requests for materials should be addressed to Alfredo Brusco, Department of Medical Sciences, University of Turin via Santena 19, 10126 Turin, Italy. *Email address:* alfredo.brusco@unito.it
A full list of authors and affiliations appears at the end of the paper.

doi: https://doi.org/10.1016/j.gim.2023.100922

gene (MIM* 138253) coding for the GluN2A regulatory subunit represent the most common event,[10,11] leading to NMDAR gain of function or loss of function and causing a wide range of epilepsies in the context of different types of NDDs.[12-14]

Synaptic transmission and plasticity at glutamatergic synapses depend on the correct synaptic localization of GluN2A-containing NMDARs.[15] Accordingly, the involvement of the GluN2A subunit in NDDs and epilepsy (MIM# 245570) has been correlated not only to aberrant receptor activation but also to altered synaptic trafficking and stabilization and balance with other NMDAR subunits for an adequate receptor functioning.[16,10] As a direct consequence, protein-protein interactions at the GluN2A C-terminal domain driving GluN2A synaptic retention have been widely investigated.[16]

GluN2A binds to scaffolding proteins of the PSD-MAGUK family (eg, PSD-95) and this interaction anchors the receptor at the postsynaptic membranes.[16] Notably, pathogenic variants in *DLG4* (MIM* 602887), the gene coding for PSD-95, have been associated with intellectual disability (ID), ASD, and epilepsy (MIM# 618793).[17,18] We previously identified Rabphilin 3A, encoded by *RPH3A* gene (MIM* 612159), as a novel GluN2A synaptic partner needed to stabilize GluN2A/PSD-95 complex at the postsynaptic density.[19] Disruption of the Rph3A/GluN2A/PSD-95 complex reduces GluN2A synaptic retention and promotes NMDARs' endocytosis.[16,19,20] *GRIN2A* and *DLG4* have been associated with rare autosomal dominant NDDs and epilepsy,[13,17,18] but so far, *RPH3A* has not been genetically associated with NDDs.

Here, we provide genetic and functional evidence for a role of *RPH3A* in NDDs.

Materials and Methods

Primary neuronal culture

Hippocampal neurons were obtained from 18-day-old rat embryos. The embryos were rapidly decapitated before the removal of tissues. Hippocampus was rapidly dissected under sterile conditions, kept in cold Hanks' balanced saline solution (4 °C) with high glucose and then digested with papain (0.5 mg/ml) dissolved in Hanks' balanced saline solution plus DNAse (0.5 mg/ml). Isolated cells were plated at a final density of 300 cells/mm^2 on plastic dishes.

Electrophysiology

Patch electrodes were fabricated from thick borosilicate glasses (Hilgenberg), pulled to a final resistance of 5 to 6 MΩ. Patch clamp recordings were performed in whole-cell configuration using a Multiclamp700-B amplifier connected to a Digidata 1440 and governed by the pClamp10 software (Axon Instruments, Molecular Devices). Experiments were performed at room temperature (22-24 °C) in whole-cell configuration and acquired with sample frequency of 10 kHz. Recordings with leak current >100pA or series resistance >20 MΩ were discarded. Analysis was performed with Clampfit software (Axon Instruments). Whole cell voltage-clamp recordings were performed at a holding potential of −70 mV. The superfused extracellular bath solution contained: 2 mM $CaCl_2$, 130 mM NaCl, 2 mM $MgCl_2$, 10 mM Hepes, 10 mM glucose, and 4 mM KCl (pH 7.4). The internal solution contained: 90 mM CsCl, 8 mM NaCl, 20 mM TEACl, 10 mM EGTA, 10 mM glucose, 1 mM $MgCl_2$, 4 mM ATP, 0.5 mM GTP, and 15 mM phosphocreatine (pH 7.4 adjusted with CsOH). For blocking synaptic currents caused by the activation of glutamatergic α-amino-3-hydroxy-5-methyl-4-isoxazolepropionic acid receptors (AMPARs) and GABAergic synapses ($GABA_A$ receptors), we added, respectively, 6,7-dinitroquinoxaline-2,3-dione, DNQX (20 μM, Sigma-Aldrich), and picrotoxin (100 μM, Sigma-Aldrich). Tetrodotoxin (TTX, 0.3 μM, Tocris Bioscience) was added to block voltage-gated Na^+ channels. The neuron was constantly superfused through a gravity system that allowed a rapid change (50-60 ms) of the solutions and the recording of I_{NMDA} after N-methyl-D-aspartate (NMDA) (50 mM) and Ifenprodil (150 nM) administration. During the experiments, NMDA was administered to neurons until I_{NMDA} reached a steady-state value. I_{NMDA} charge was measured as the area under 8 seconds of whole-cell current. GluN2B-mediated component was calculated as the difference between total NMDA current and GluN2A-dependent current measured in the presence of Ifenprodil (150 nM).

Immunocytochemistry

For colocalization and morphological studies, transfected hippocampal neurons were fixed for 10 minutes at room temperature in 4% paraformaldehyde and 4% sucrose in Dulbecco's phosphate buffered saline (PBS). Coverslips were then washed with PBS, permeabilized with 0.1% Triton X-100 in PBS for 15 minutes at room temperature and blocked for 30 minutes at room temperature with 5% bovine serum albumin (BSA) in PBS. Cells were then incubated with primary antibodies in 5% BSA-PBS overnight at 4 °C in a humidified chamber. After washing with PBS, the cells were incubated with the fluorophore-conjugated secondary antibodies in 5% BSA-PBS for 1 hour at room temperature in a humidified chamber protected from light. The incubation was followed by washing with PBS and mounting onto glass slides using Fluoroshield mounting medium (Sigma-Aldrich).

Surface staining assays were performed as previously reported with few modifications.[19,20] Transfected hippocampal neurons were fixed for 10 minutes at room temperature in 4% paraformaldehyde and 4% sucrose in Dulbecco's PBS. Coverslips were washed with PBS and then blocked for 30 minutes at room temperature with 5% BSA in PBS. Cells were not permeabilized and were labeled

for 1 hour at room temperature with primary antibodies (anti-GluN2A or anti-GluA1) recognizing an extracellular epitope at N-terminal region of the subunits. This procedure allows for surface staining by targeting the epitope in the extracellular domain. The coverslips were then washed in PBS and a secondary antibody conjugated to Alexa Fluor dye was used. The coverslips were then washed with PBS, permeabilized with 0.1% Triton X-100 in PBS for 15 minutes and blocked for 30 minutes at room temperature with 5% BSA in PBS. Cells were then incubated with the same primary antibodies in 5% BSA-PBS for 1 hour at 4 °C in a humidified chamber. After washes with PBS, the cells were incubated with the fluorophore-conjugated secondary antibodies in 5% BSA-PBS for 1 hour in a humidified chamber protected from light. The incubation was followed by washing with PBS and mounting onto glass slides using Fluoroshield mounting medium (Sigma-Aldrich).

Confocal imaging

Images were taken using LSM900 (Zeiss) confocal microscopes with 63× objective at a 0.09 µm pixel size and analyzed using ImageJ software. Cells were randomly chosen for quantification from different coverslips from independent experiments and images were acquired using the same settings and laser power. Z-stack images were taken with a Z-step of 0.35 µm, and analyses were performed with ImageJ.

For each dendritic spine, length, head, and neck width were measured, which was used to classify dendritic spines into 3 categories (thin, stubby, and mushroom). In particular, the length and the ratio between the width of head and the width of neck (Wh/Wn) were used as parameters for the classification as follows: protrusions having a length of more than 3 µm were considered as filopodia, the others as spines; spines with a Wh/Wn ratio bigger than 1.7 were considered mushrooms; and spines with a Wh/Wn ratio smaller than 1.7 were divided into stubby, if shorter than 1 µm, and thin, if longer than 1 µm. Protrusions with length over 5 µm were excluded from the analysis. For each neuron, a total length of about 150 to 200 µm of proximal dendrites and 100 to 150 dendritic spines were considered. For super-resolution assays, images were taken using the Airyscan mode on a LSM900 confocal microscope (Zeiss) with a 63× objective at a 0.04 mm pixel size.

Analysis of GCaMP7 signals

Calcium imaging experiments using pCAG_Xph20-GCaMP7f calcium indicator were performed in primary hippocampal neuronal cultures at DIV16. pCAG_Xph20-GCaMP7f was a gift from Matthieu Sainlos (Addgene plasmid #135539; http://n2t.net/addgene:135539; RRID: Addgene_135539). Live-cell imaging acquisition was performed using an LSM900 (Zeiss) confocal microscopes with 63× objective. Dendrites were imaged in artificial cerebral spinal fluid (ACSF) at 37 ºC in an atmosphere of 5% CO_2 at maximum scanning speed with 6.7 zoom (scan time around 35 ms, resolution: 0.07 nm/pixel) and time-lapse images were taken for 3 minutes at 10 Hz. For quantitative analysis, dendritic spines were chosen as regions of interest, and the GCaMP7f fluorescence was plotted over time using ImageJ. For each region of interest, we computed the number of every calcium transient event showing a ΔF/Fmin over 0.5 in a time window of 3 minutes, and the area under the ΔF/Fmin curve, with Fmin being the baseline value of fluorescent intensity.

Results

Identification of patients with variants in RPH3A

We examined trio-based exome sequencing data from 538 individuals diagnosed with NDDs in local hospitals, within the Autism Sequencing Consortium project[5,21] for any rare *RPH3A* variants not seen in Genome Aggregation Database (gnomAD)[22] or de novo. Written informed consent for genetic testing and permission for publication of the clinical data was obtained from all individuals and/or their legal representatives by the referring physicians, according to the guidelines of the ethics committees and institutional review boards of the respective institutes. We identified a male individual (case #1) with a de novo *RPH3A* variant (NM_001143854.2: c.1853A>G, p.(Asn618Ser)) and high-functioning ASD, mild ID, dysgraphia, hyperactivity, increased body weight, and abnormal facial features (Supplemental note: clinical reports). Querying the GeneMatcher platform,[23] we identified 2 additional male individuals carrying de novo *RPH3A* missense variants c.219G>T p.(Gln73His) (case #2) and c.1349C>G (p.Thr450Ser) (case #3; ClinVar SCV000265605.3). They both showed a different neurodevelopmental phenotype with epilepsy, moderate ID, and hypotonia. Array-CGH and Fragile-X syndrome testing were negative for all individuals.

Finally, by searching the Exomiser-based candidate variants from the individuals with clinical indications "intellectual disability" (n = 6203) and "epilepsy plus other features" (n = 1362) in the 100,000 Genomes Project,[24] we identified 3 additional males with missense variants in *RPH3A*: c.626G>A; p.(Arg209Lys) (case #4), c.705G>T; p.(Arg235Ser) (case #5), and c.1524G>C; p.(Gln508His) (case #6) (Figure 1A). Parents of cases #4 and #5 were not available for segregation analysis. The mother of case #6 did not to carry the p.(Gln508His) variant, his father was not available. Clinically, cases #4 and #6 showed drug-resistant epilepsy and moderate ID, similar to cases #2 and #3. Case #5 showed childhood ASD, ID, and obesity, similar to case #1. Further clinical details are provided in supplemental material.

The Exomiser-based analysis revealed an additional male with the c.444G>T change, which is predicted to cause a

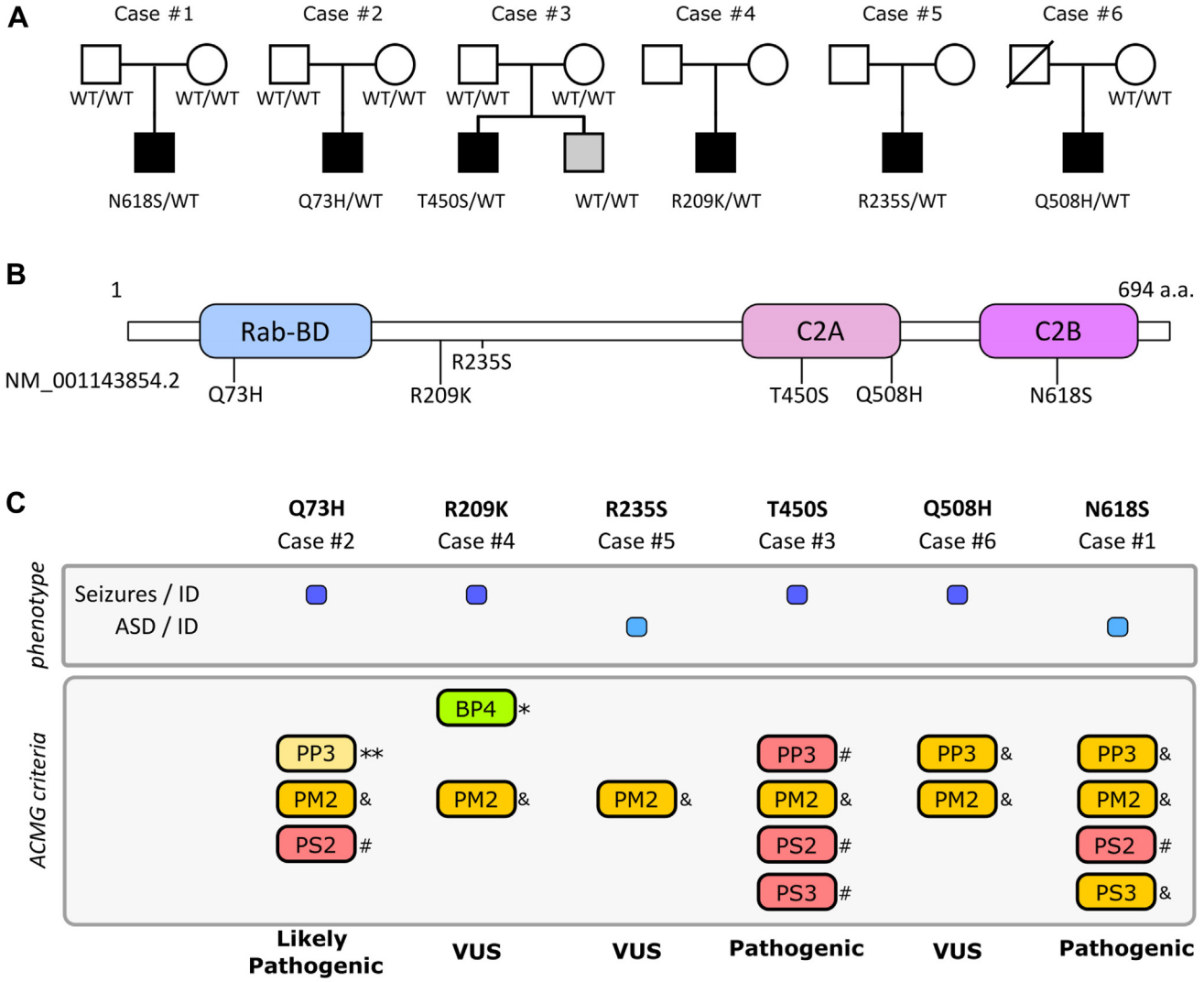

Figure 1 ***RPH3A* variants in 6 individuals.** A. Pedigrees of the 6 identified *RPH3A* variants; affected probands (all males) are indicated with full black squares. For cases #1, #2, and #3, parents were available, and the variants were proven to be de novo. Case #3 was reported to have a younger brother (gray) affected by a disorder partially overlapping with the one of the probands, except for epilepsy. He did not carry the *RPH3A* variant. Additional details are provided in Supplemental materials. B. Schematic representation of RPH3A protein, based on InterPro data (http://www.ebi.ac.uk/interpro/), is shown. The Rab-binding domain (Rab-BD, amino acids 44-160), and the 2 C2 domains (C2A, amino acids 392-514; C2B, amino acids 550-683) are indicated. The *RPH3A* (NM_001143854.2) variants described in the present work are represented along the protein. C. The phenotype associated with the reported variants is schematized (ID = intellectual disability; ASD = autism spectrum disorder), together with the ACMG criteria[7] applied and its final classification. Different colors/symbols of the panels indicate the strength of each applied criteria: "benign supporting" - "moderate" in green (*); "pathogenic supporting" - "supporting" in light yellow (**), "moderate" in orange (&), "strong" in red (#). PP3: multiple lines of computational evidence support a deleterious effect on the gene/gene product; PM2: absent in population databases; PS2: de novo (paternity and maternity confirmed); PS3: well-established functional studies show a deleterious effect; BP4: multiple lines of computational evidence suggest no impact on the gene or gene product. ACMG, American College of Medical Genetics and Genomics; VUS, variant of uncertain significance; WT, wild-type.

Glu148Asp substitution. This variant affects the last nucleotide of exon 7 and is expected to cause an alteration of splicing with 72 bp intron retention and a premature stop codon (Supplemental Figure 2). Because haploinsufficiency of *RPH3A* is not likely leading to disease (see discussion, GnomAD pLI = 0[22,25]), we excluded this case from our survey.

All the identified missense variants were absent from the GnomAD (v2.1.1[22]), and 4 of 6 were in known functional domain of the protein (Figure 1B). The American College of Medical Genetics and Genomics classification was used applying the criteria shown in Figure 1C, resulting in 3 variants classified as variant of uncertain significance (p.(Arg209Lys), p.(Arg235Ser), and p.(Gln508His)), 1 as likely pathogenic (p.(Gln73His)) and 2 as pathogenic (p.(Thr450Ser) and p.(Asn618Ser)). Bioinformatic predictions were not concordant in the pathogenicity scores (see Supplemental Table 1): for instance, Combined

Annotation Dependent Depletion (CADD) score was below 20 for variants in position 209 and 235; further details are provided in Supplemental Table 1. Of note, c.1853A>G p.(Asn618Ser) is 5 bases upstream of the intron 20 splice donor site, but we excluded a possible impact on mRNA processing by minigene assay (Supplemental Figure 3).[26]

In silico evaluation of identified variants

To explore the functional effect of the *RPH3A* variants, we modeled in silico 4 variants localized in key domains of the protein and associated with different phenotypes: p.(Gln73His) (hereby indicated as hRPH3A^{Q73H}), p.(Thr450Ser) (hereby indicated as hRPH3A^{T450S}), p.(Gln508His) (hereby indicated as hRPH3A^{Q508H}), and p.(Asn618Ser) (hereby indicated as hRPH3A^{N618S}) (Figure 2). It was not possible to analyze the variants p.(Arg209Lys) and p.(Arg235Ser) because they are located in a disordered region of RPH3A that could not be modeled. hRPH3A^{Q73H} is located in the Rab binding domain; the impact of the substitution of an His with a Gln on the overall hRPH3A^{Q73H} stability is predicted to be minimal, as the $\Delta\Delta G$ increased by approximately 1.5 kcal/mol. Histidine perfectly replaces glutamine side chains, establishing the same interactions with Gln69 and Gly77 plus a weak H-bond interaction with Gly154 that potentially affects the dynamics and the molecular recognition mechanism of its Rab binding domain (Figure 2A and B).

hRPH3A^{T450S}, hRPH3A^{Q508H}, and hRPH3A^{N618S} affect residues located within the C2A and C2B protein domains, which play a fundamental role in the regulation of activity-dependent protein function at the postsynaptic compartment.[27,28] Using 2 crystallographic structures of *Rattus norvegicus* Rph3A (PDB ID: 4LT7 for the C2A domain; PDB ID: 2CM6 for the C2B domain),[3,4] we first built three-dimensional models of hRPH3A^{WT} and then generated variants. Moreover, the experimentally solved structure of *Mus musculus* Rph3A (PDB ID: 2K3H)[29] was carefully considered to evaluate the side-chain orientations of residues near to Thr450 and Ca^{2+} ions. The 2K3H structure contains 20 conformers solved by nuclear magnetic resonance.[29] We observed that the carboxyl group of Glu472 was close to Asn481 in only 4 conformers, whereas the carboxyl group of Glu472 is closed to Thr437 in the remaining 16, similar to what occurs in the 4LT7 crystallographic structure. hRPH3A^{WT} showed the same local interaction network of the mouse and rat proteins: the carboxyl group of Glu485 forms a hydrogen bond with the hydroxy group of Thr450, and the backbone of Glu485 cooperates with Leu427, Asp429, Asp486, and Asp487 in binding 1 Ca^{2+} ion. The impact of the Thr-to-Ser substitution on the overall hRPH3A^{T450S} stability is predicted to be minimal, as the stability scoring function ($\Delta\Delta G_s$) increased by approximately 1.3 kcal/mol. On the other hand, a comparative analysis of orientations of amino acid side chains (rotamer) between the hRPH3A^{WT} and hRPH3A^{T450S} structures suggested a different local stability of Thr and Ser rotamers positioned at 450. Different rotamers can cause changes in the local interaction network, affecting protein structure and functions. Threonine 450 is characterized just by 1 stable rotamer, forming a hydrogen bond with the side chain of Glu485; differently, the most stable serine 450 rotamer, with a minimum energy value (~3.5 kcal/mol) lower than that of other Ser rotamers, is not able to interact with Glu485, strongly affecting the interaction network of the residues that directly interact with Ca^{2+} ions (Figure 2C and D). The change of this interaction network was expected to alter the C2A affinity to inositol-1,4,5-trisphosphate (IP3), inhibiting protein recruitment in the membrane. In fact, the C2A domain of RPH3A binds IP3 in a Ca^{2+}-dependent manner, with an affinity in the micromolar range in presence of saturating concentration of Ca^{2+}.[29] hRPH3A^{Q508H} change increased the $\Delta\Delta G_s$ by approximately 1.4. kcal/mol. This variant is located on the surface of the C2A domain, but it could also interact with other RPH3A domains or other proteins that were not considered in our 3D modeling (Figure 2E and F). Finally, hRPH3A^{N618S} does not significantly reduce protein stability, increasing the $\Delta\Delta G_s$ by just approximately 0.6 kcal/mol. This variant locally decreases the hydrophobic surface area by about 10 Å^2 (Figure 2D) and the overall protein volume by about 26 Å.[3] These effects depend upon the interaction network of Glu616, which establishes a hydrogen bond with Arg573 and residue 618 in both hRPH3A^{WT} and hRPH3A^{N618S}. Although Ser618 maintains the same interaction network of Asn618, its side chain is shorter, causing a contraction of the total protein volume (Figure 2G and H).

Rph3A variants cause increase of total and GluN2A-dependent NMDA currents

To evaluate whether the p.(Thr450Ser) and p.(Asn618Ser) substitutions could affect NMDAR function, we examined NMDAR currents (I_{NMDA})[30,31] via whole-cell patch clamp recordings on rat hippocampal neuronal cultures.[32] To perform experiments, we took advantage of a mouse hSyn-RFP-Rph3A-WPRE plasmid,[20] mutagenized in position 437 (corresponding to human 450) or 605 (corresponding to human 618; multiple alignment information is reported in Supplemental Figure 4). Specifically, we compared the I_{NMDA} amplitudes by bath application of exogenous NMDA in RFP-Rph3A^{WT} versus RFP-Rph3A^{T437S} or RFP-Rph3A^{N605S} transfected neurons (Figure 3A). Neurons were transfected at day in vitro 8 (DIV8) and all recordings were performed at DIV16. Whole-cell recordings were performed by holding membrane potential at −70 mV. Exogenous application of NMDA (50 μM) induced a mean I_{NMDA} amplitude of 283.3 ± 28.23 pA in neurons expressing RFP-Rph3A^{WT}, which significantly increased in neurons expressing either variant (RFP-Rph3A^{T437S}, 602.75 ± 68.79 pA, $P < .0001$; RFP-Rph3A^{N605S}, 590.33 ± 79.03 pA, $P < .01$) (Figure 3C). Thus, these results indicate that Rph3A variants can produce an increase either in the number of NMDARs on the membrane surface or in their conductance.

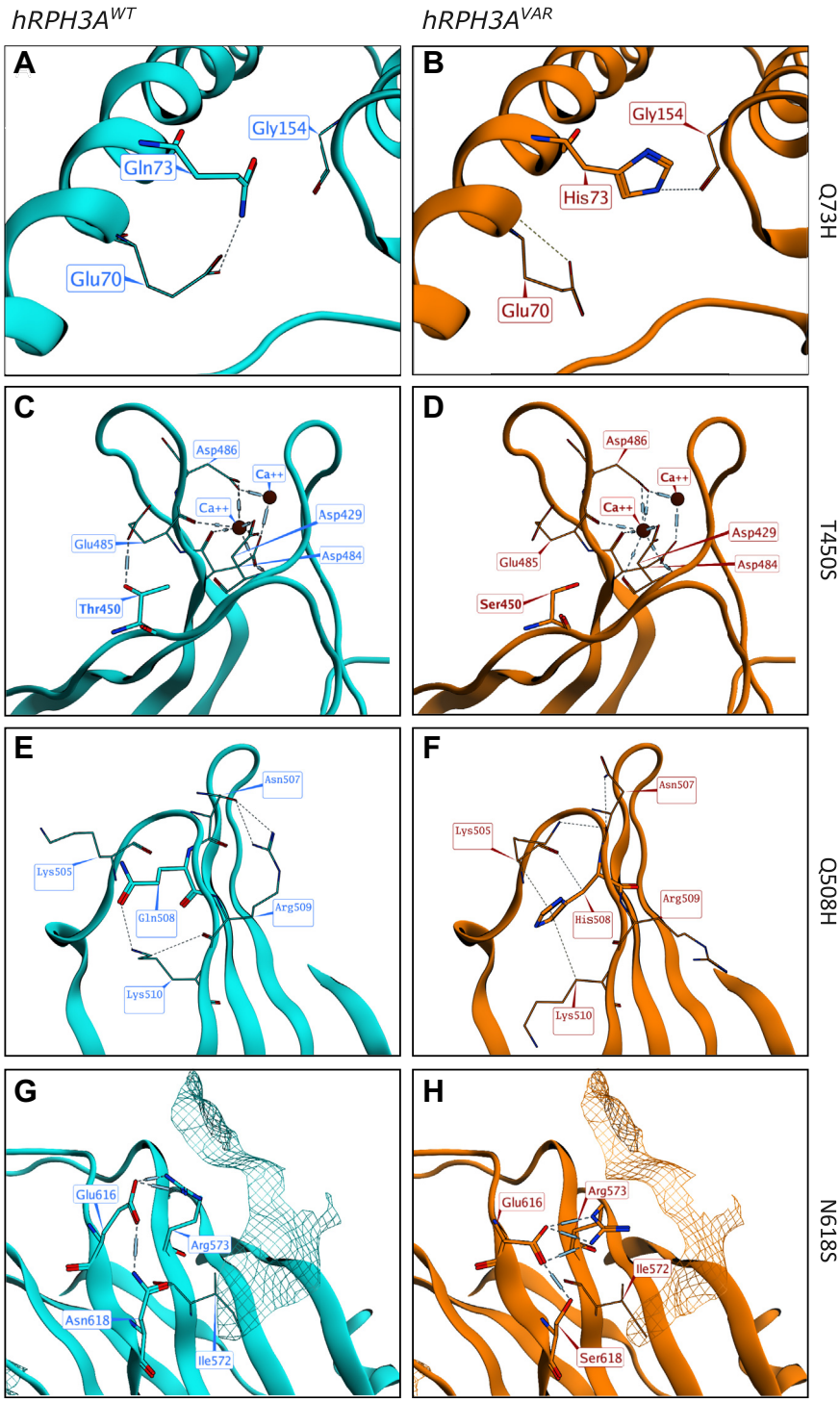

Figure 2 ***h*RPH3A protein conformation *in silico* analysis.** In silico conformation analyses of the wild-type (hRPH3A^{WT}) and variant (hRPH3A^{VAR}) forms of human rabphilin are reported. A-B. The Rab-BD domain of hRPH3A^{WT} vs hRPH3A^{Q73H} is shown. In the hRPH3A^{WT}, Gln73 interact with Glu70, whereas in hRPH3A^{Q73H} His73 interact with Gly154 instead of Glu70, likely reducing domain flexibility. C-D. The C2A domain of hRPH3A^{WT} vs hRPH3A^{T450S} is shown. The interaction network of Ca^{2+} involving Asp484, Glu485, Asp429, Asp486, and Thr450 is shown for hRPH3A^{WT}. Notably, the network of Ca^{2+} for hRPH3A^{T450S} involves the same residues but not Ser450, because of the loss of the hydrogen bond with the side chain of Glu485. This event has an important effect on the interaction network of the residues directly interacting with the Ca^{2+} ions. E-F. The C2B domain of hRPH3A^{WT} vs hRPH3A^{Q508H}. The interaction network in hRPH3A^{WT} involves Gln508, Lys510 and Arg509, whereas the interaction network in hRPH3A^{Q508H} involves His508, Lys 510, and Lys505 instead of Arg509. G-H. The C2B domain of hRPH3A^{WT} vs hRPH3A^{N618S} is involved in an interaction network that involves Glu616, which establishes a hydrogen bond with Arg573 and residue Asn618. The network is not impaired for Ser618; however, because the side chain of Ser618 is shorter than the Asn618 one, the total protein volume is reduced.

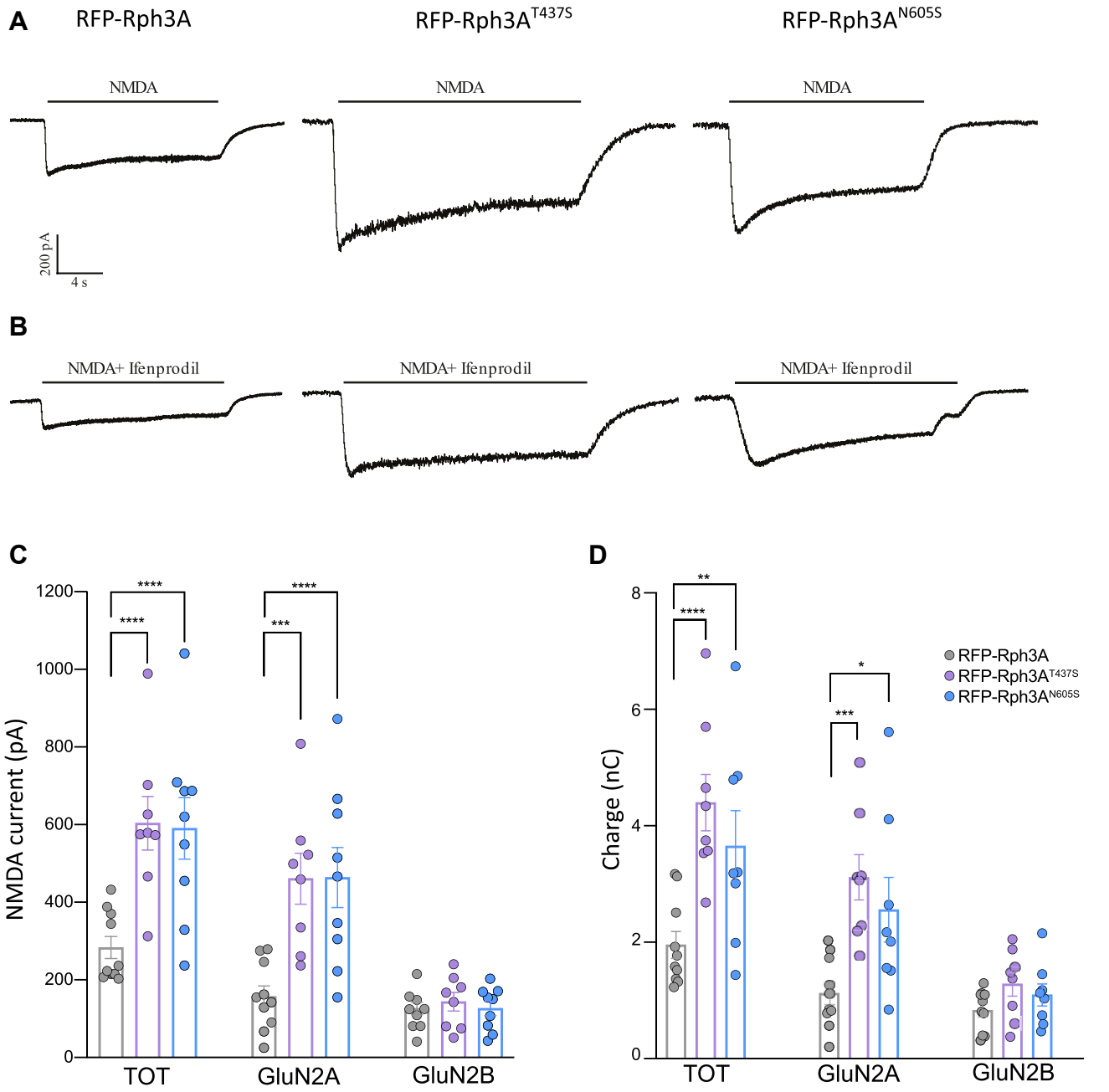

Figure 3 **Rph3A^{T437S} and Rph3A^{N605S} increase total and GluN2A-dependent NMDA currents.** A. Representative traces of whole-cell responses to NMDA (50 mM) in Rph3A^{WT}, Rph3A^{T437S}, and Rph3A^{N605S} neurons show an increase of I_{NMDA} amplitude when cells are transfected with Rph3a variants. B. Representative traces of whole-cell responses to NMDA (50 mM) and Ifenprodil (150 nM) in Rph3A^{WT}, Rph3A^{T437S} and Rph3A^{N605S} transfected neurons show that there is a 45% inhibition of I_{NMDA} in neurons overexpressing RFP-Rph3A^{WT}, whereas neurons expressing RFP-Rph3A^{T437S} and Rph3A^{N605S} showed a 24% and 21% inhibition, respectively. C-D. Representative bar graphs of total, GluN2A, and GluN2B-mediated NMDA current (C) and charge (D). RFP-Rph3A^{WT} (n = 10); RFP-Rph3A^{T437S} (n = 9); Rph3A^{N605S} (n = 8). Two-way ANOVA. ANOVA, analysis of variance; NMDA, N-methyl-D-aspartate.

In mature hippocampal neurons NMDA whole-cell currents depend mostly on GluN2A and GluN2B components.[31,32] Therefore, we investigated the specific contribution of GluN2A to the total currents by using ifenprodil (Figure 3B), a noncompetitive GluN2B inhibitor. In the presence of ifenprodil (150 nM), we observed a 45% inhibition of I_{NMDA} in neurons overexpressing RFP-Rph3A^{WT}, in line with previous observations.[20] In contrast, a lower reduction of I_{NMDA} amplitude was observed in neurons expressing the RFP-Rph3A^{T437S} or Rph3A^{N605S} variants (24% and 21%, respectively). Particularly, the mean GluN2A-mediated currents were significantly higher in neurons expressing RFP-Rph3A^{T437S} or RFP-Rph3A^{N605S} than those in control neurons (I_{NMDA} RFP-Rph3A^{WT}: 157.03 ± 27.44 pA; RFP-Rph3A^{T437S}: 460.01 ±

65.63 pA, $P < .001$; RFP-Rph3A^{N605S}: 463.89 ± 77.28 pA, $P < .0001$) (Figure 3C), whereas the mean GluN2B-dependent current did not show differences between groups (Figure 3C). To further validate these results and exclude any effects produced by changes of the deactivation kinetic of I_{NMDA}, we next assessed the charge underlying I_{NMDA} (Figure 3D). We found that I_{NMDA} charge in neurons expressing RFP-Rph3A^{T437S} or RFP-Rph3A^{N605S} was increased compared with neurons overexpressing the wild-type protein (RFP-Rph3A^{WT}: 1.95 ± 0.23 nC; RFP-Rph3A^{T437S}: 4.40 ± 0.48 nC, $P < .01$; RFP-Rph3A^{N605S}: 3.65 ± 0.60 nC, $P < .0001$). The I_{NMDA} charge dependent on GluN2A subunits was significantly higher in neurons expressing RFP-Rph3A^{T437S} and RFP-Rph3A^{N605S} variants than in control neurons (RFP-Rph3A^{WT}: 1.12 ± 189.01 nC; RFP-Rph3A^{T437S}: 3.11 ± 0.40 nC, $P < .001$; RFP-Rph3A^{N605S}: 2.56 ± 0.56 nC; $P < .05$) (Figure 3D). Overall, these data show an increased activity of GluN2A-containing NMDARs in Rph3A^{T437S} and Rph3A^{N605S} variants, suggesting higher levels of GluN2A-containing NMDARs at the membrane.

NMDAR-GluN2A localization and availability are affected by Rph3A variants

To directly test this hypothesis, we evaluated GluN2A surface levels in the dendrites of rat primary hippocampal neurons. We overexpressed RFP-Rph3A^{WT}, RFP-Rph3A^{N605S}, or RFP-Rph3A^{T437S} in hippocampal neurons by transfection at DIV8, and the endogenous GluN2A surface level was analyzed at DIV16 normalized to the total level of GluN2A. As shown in Figure 4A and B, overexpression of RFP-Rph3A^{T437S} induced a significant increase of GluN2A surface levels in dendrites compared with neurons overexpressing RFP-Rph3A^{WT} ($P < .01$, Rph3A^{T437S} vs Rph3A^{WT}), whereas RFP-Rph3A^{N605S} did not modify GluN2A surface availability ($P = .68$, Rph3A^{N605S} vs Rph3A^{WT}).

NMDA receptors are highly mobile and can be localized both at synaptic and extrasynaptic sites, depending upon subunit composition. Stimulation of synaptic NMDARs promotes cell survival, whereas the stimulation of extrasynaptic receptors results in neurotoxicity and can trigger intracellular pathways leading to cell death.[1,32] To test whether the *RPH3A* variants alter NMDAR synaptic retention, we examined the colocalization of GluN2A with PSD-95, the main scaffolding protein of the excitatory postsynaptic density involved in the physiological synaptic localization of NMDARs.[1,16] RFP-Rph3A^{WT}, RFP-Rph3A^{N605S}, or RFP-Rph3A^{T437S} were overexpressed in hippocampal neurons at DIV8 and then immunocytochemistry assay for GluN2A and PSD-95 was performed at DIV16. Confocal microscopy with Airyscan super-resolution module was used to identify co-localization puncta. As shown in Figure 4C and D, the percentage of GluN2A co-localizing with PSD-95 was decreased in neurons expressing either variant ($P < .0001$, Rph3A^{N605S} vs Rph3A^{WT}; $P < .01$, Rph3A^{T437S} vs Rph3A^{WT}).

Variants of Rph3A affect postsynaptic calcium currents

To assess whether reduced GluN2A synaptic localization in Rph3A variant neurons was associated with altered postsynaptic calcium levels, we used the novel genetically encoded calcium-sensing probe pCAG_Xph20-GCaMP7f containing the Xph20 moiety for specific and efficient binding to endogenous PSD-95. This approach allows for the specific evaluation of calcium transients at dendritic spines using live imaging. As shown in Figure 4E, neurons overexpressing Rph3A^{N605S} or Rph3A^{T437S} were characterized at rest by an alteration of postsynaptic calcium transients. Rph3A^{T437S} was characterized by lower area under the curve of calcium signals compared with neurons expressing Rph3A^{WT} (Figure 4F, $P < .01$, Rph3A^{T437S} vs Rph3A^{WT}), whereas Rph3A^{N605S} showed a reduction of number of calcium events (Figure 4G; $P < .01$, Rph3A^{N605S} vs Rph3A^{WT}).

Rph3a^{T437S} affects dendritic spines' morphology

Rph3A can interact with MyosinVA.[33] Because MyosinVA acts as motor protein transporting GluA1-containing AMPARs in dendritic spines,[34] Rph3A variants might alter the membrane insertion of AMPARs during synaptic plasticity events, thus affecting dendritic spines morphology. Therefore, we quantified the level of AMPARs on the membrane by analyzing the GluA1 subunit surface availability in the dendrites of hippocampal neurons. As shown in Figure 5A and B, the analysis of GluA1 surface levels did not show any significant differences among the 3 experimental groups, suggesting that *RPH3A* variants only affect NMDA-type ionotropic glutamate receptors. Excitatory neurotransmission strictly modulates dendritic spine morphology and density, reflecting specific states of the synapse. Notably, Rph3A synaptic activity has been closely correlated to modifications of dendritic spine density.[16,19,20] Based on these data, we investigated the impact of Rph3A on dendritic spine formation and maturation by examining their density and morphology. To this end, hippocampal primary neurons were co-transfected with GFP and RFP-Rph3A^{WT}, RFP-Rph3A^{N605S}, and RFP-Rph3A^{T437S} and then analyzed for evaluation of dendritic spine density and shape. We did not observe any significant change in dendritic spine density (Figure 5C and D). For a more detailed morphological analysis, the dendritic spine length, head width, and neck width were measured and spines were categorized within the filopodia, mushroom, stubby, and thin classes (Figure 5E-H). No differences were found in the length of spines (Figure 5E) or percentage of filopodia (Figure 5G). However, a significant reduction of head width was associated with the Rph3A^{T437S} variant ($P < .05$, Rph3A^{T437S} vs Rph3A^{WT}) (Figure 5F). Accordingly, the number of thin spines of neurons overexpressing Rph3A^{T437S} were significantly increased compared with the

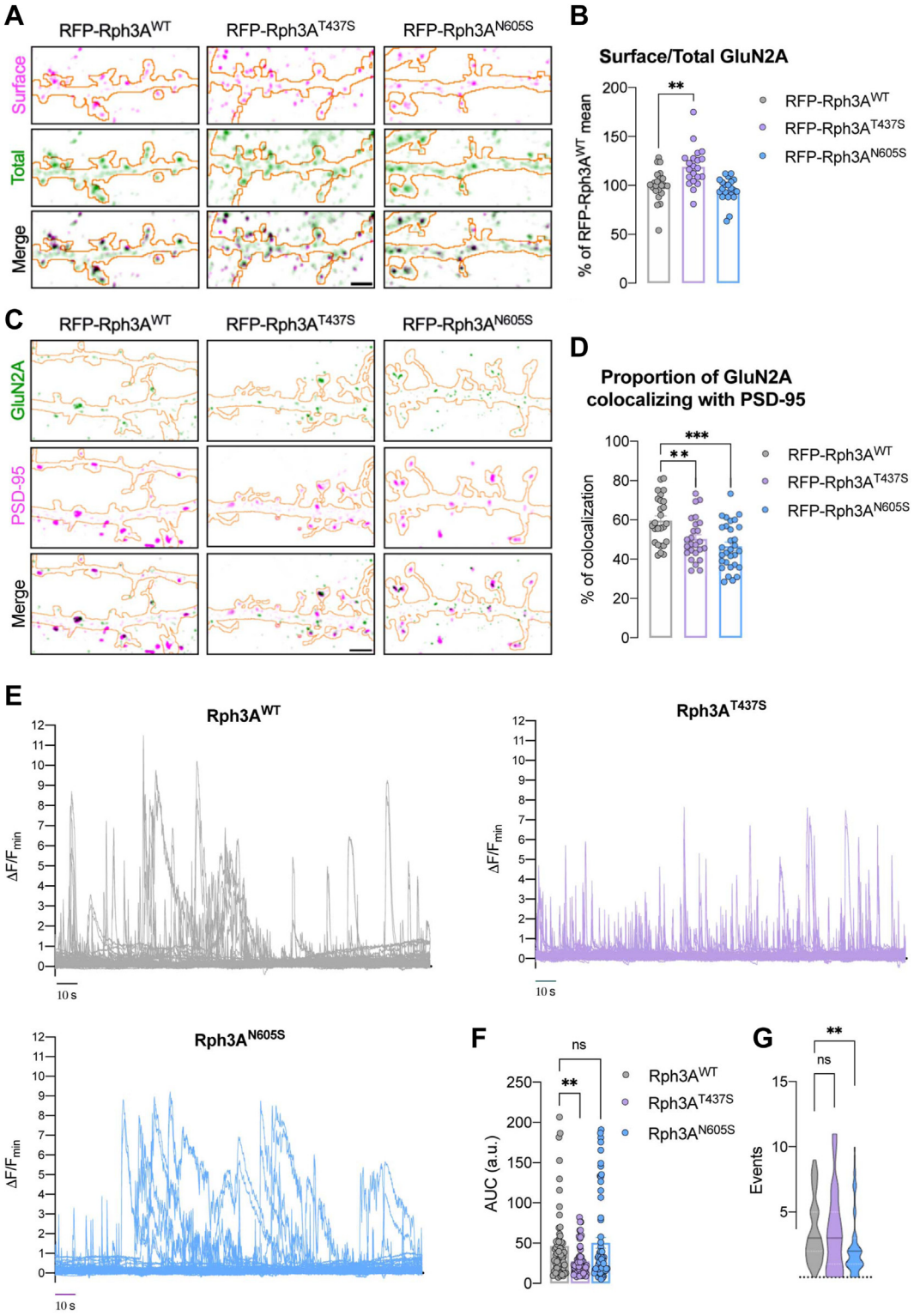

Figure 4 **The localization, availability, and postsynaptic calcium currents of GluN2A are impaired by Rph3A variants.** A. Confocal images of surface (magenta) and total GluN2A (green) staining in RFP-Rph3A^{WT}, RFP-Rph3A^{N605S}, or RFP-Rph3A^{T437S} transfected neurons (outlined in orange). Scale bar: 2 μm. B. A bar graph representing the mean ± SEM of the percentage of RFP-Rph3A^{WT} mean GluN2A surface/total ratio was analyzed using a Kruskal-Wallis test with Dunn's post hoc test. $^{**}P < .01$. The dots represent single values. C. Airyscan confocal images of GluN2A (green) and PSD-95 (magenta) staining in RFP-Rph3A^{WT}, RFP-Rph3A^{N605S}, or RFP-Rph3A^{T437S} transfected neurons (orange outline). Scale bar: 2 μm. D. A bar graph representing the mean ± SEM of the percentage of GluN2A colocalizing with PSD-95 was analyzed using an ordinary one-way ANOVA with Dunnett's post hoc test. $^{***}P < .0001$, $^{**}P < .01$. Dots represent single values. E. Xph20-GCaMP7f fluorescent signals over time (3 min) in DIV16 primary hippocampal neurons transfected at DIV8 with RFP-Rph3A^{WT}, RFP-Rph3A^{N605S}, or RFP-Rph3A^{T437S}. F. A bar graph representing the mean ± SEM of the area under the curve

number of thin spines of neurons overexpressing Rph3A^{WT} ($P < .05$, Rph3A^{T437S} vs Rph3A^{WT}) (Figure 5H). Overall, these results indicate that, at least in the present experimental conditions, only the p.(Thr437Ser) change induces spine morphology changes.

Discussion

RPH3A, encoding for the synaptic protein Rabphilin 3A, participates in the NMDARs complex, which is essential for synaptic plasticity and cognition.[1] Because the synaptic excitation/inhibition balance is one of the most well-known pathways associated with NDDs, *RPH3A* was a strong candidate for these diseases. However, *RPH3A* previously only had suggestive evidence of an association with human disease. Compound heterozygous variants affecting residues 269 and 464 were reported in an individual with congenital myasthenic syndrome, although the functional and clinical relevance of those changes has not been firmly established.[35] We analyzed the variant p.(Val464Leu) in silico, showing that it localizes on the protein surface and may affect the C2B domain interactions with other RPH3A binding partners and induce a local unfolding of a β-strand (Supplemental Figure 5). However, testing of the variant in position 269 was not possible because of the localization in a disordered region, and it is therefore intricate to hypothesize the effect of the combination of the 2 variants. More recently, about 2 Mb region encompassing *RPH3A* has been reported as a novel epilepsy-risk region, hosting multiple epilepsy-associated single-nucleotide variations affecting *RPH3A* expression.[36]

Here, we described 6 cases with missense variants in *RPH3A* [p.(Gln73His)*dn*; p.(Arg209Lys); p.(Arg235Ser); p.(Thr450Ser)*dn*; p.(Gln508His); p.(Asn618Ser)*dn*] showing either drug-resistant epilepsy and ID (Cases #2, #3, #4, and #6) or high functioning ASD and learning disability (Cases #1 and #5). Case #3 also had additional features, including language and motor impairment, breathing issues, and mixed hypo/hypertonia. Indeed, he also carried variants in the *CUL4B*, *PRKAG2*, and *SCN4A* genes that could likely explain his clinical variability and features, such as motor impairment and language impairment. None of these genes had been linked to seizures, thus making *RPH3A* the most likely candidate for epilepsy. Hypotonia has been reported also for case #2, suggesting that this could be also partially associated with the variant in *RPH3A*.

Using in vitro cellular models, we proved the p.(Thr450Ser) amino acid substitution leads to widespread alterations in hippocampal neurons, including aberrant activation of NMDARs, alterations of GluN2A synaptic localization, and surface levels and dynamics of calcium transients at dendritic spines. These molecular and functional events are also associated with the presence of thinner dendritic spines. In addition, structural analysis shows an impact of p.(Thr450Ser) on the interaction network of the residues directly interacting with Ca^{2+} ions. The p.(Asn618Ser) amino acid substitution displayed similar alterations, though GluN2A surface levels and dendritic spine morphology were not affected. Importantly, both RPH3A^{T450S} and RPH3A^{N618S} did not induce alterations of AMPARs, suggesting a specific effect on NMDA receptors. Our data agree with previous studies, indicating that a balanced Rph3A activity at the synaptic NMDAR complex is needed for the induction of synaptic plasticity and NMDAR-dependent behaviors.[16,20] The altered synaptic retention of GluN2A-containing NMDARs observed here in neurons transfected with both Rph3A^{T450S} and Rph3A^{N618S} suggests that their stimulation can promote pathological glutamatergic events, known to be mostly associated with extrasynaptic NMDARs.[1,15] Importantly, aberrant Rph3A interactions with GluN2A-containing NMDARs have been previously observed in models of pathological synaptic plasticity, such as parkinsonian rats displaying a dyskinetic profile.[37]

Beyond p.(Thr450Ser) and p.(Asn618Ser) variants, we identified p.(Glu73His) as likely pathogenic and p.(Arg209Lys), p.(Arg235Ser), and p.(Glu508His) as variants of uncertain significance.

A loss-of-function pathogenic mechanism for the *RPH3A* missense variants reported here is unlikely: haploinsufficiency scores are compatible with a recessive gene (pLI: 0; LOEUF: 0.47),[22,25] and mice lacking *Rph3a* are viable and show no gross alterations.[38] For these reasons, we excluded from our analysis a case carrying the c.444G>T splicing variant because it is predicted to cause the insertion of a premature stop codon. Our experiments suggest that the 2 studied variants, p.(Thr437Ser) and p.(Asn605Ser), have a functional gain of function, with increased GluN2A-mediated NMDAR currents and extrasynaptic GluN2A availability on the membrane, as well as enhanced postsynaptic calcium transients. It is plausible to hypothesize that different missense variants may have variable impact on Rph3A function, depending on their localization along the protein. Additional numbers and data are required to determine increased susceptibility among males. The identification of additional subjects with pathogenic variants in this gene is expected to provide a more accurate picture of the clinical variability and genotype-phenotype correlations associated with altered RPH3A function.

In conclusion, here, we provide evidence of a causal association between missense variants in the *RPH3A* gene

of spontaneous calcium transient events (evaluated as changes of Xph20-GCaMP7f fluorescence) at RFP-Rph3A^{WT}, RFP-Rph3A^{N605S}, and RFP-Rph3A^{T437S} dendritic spine over 3 min, Kruskal-Wallis test with Dunn's *post hoc* test. G. Violin plot representing the number of events per spine over a 3-min period was tested using Kruskal-Wallis' test with Dunn's post hoc test. Black lines represent the mean, and white dotted lines represent quartiles. ANOVA, analysis of variance; SEM, standard error of the mean.

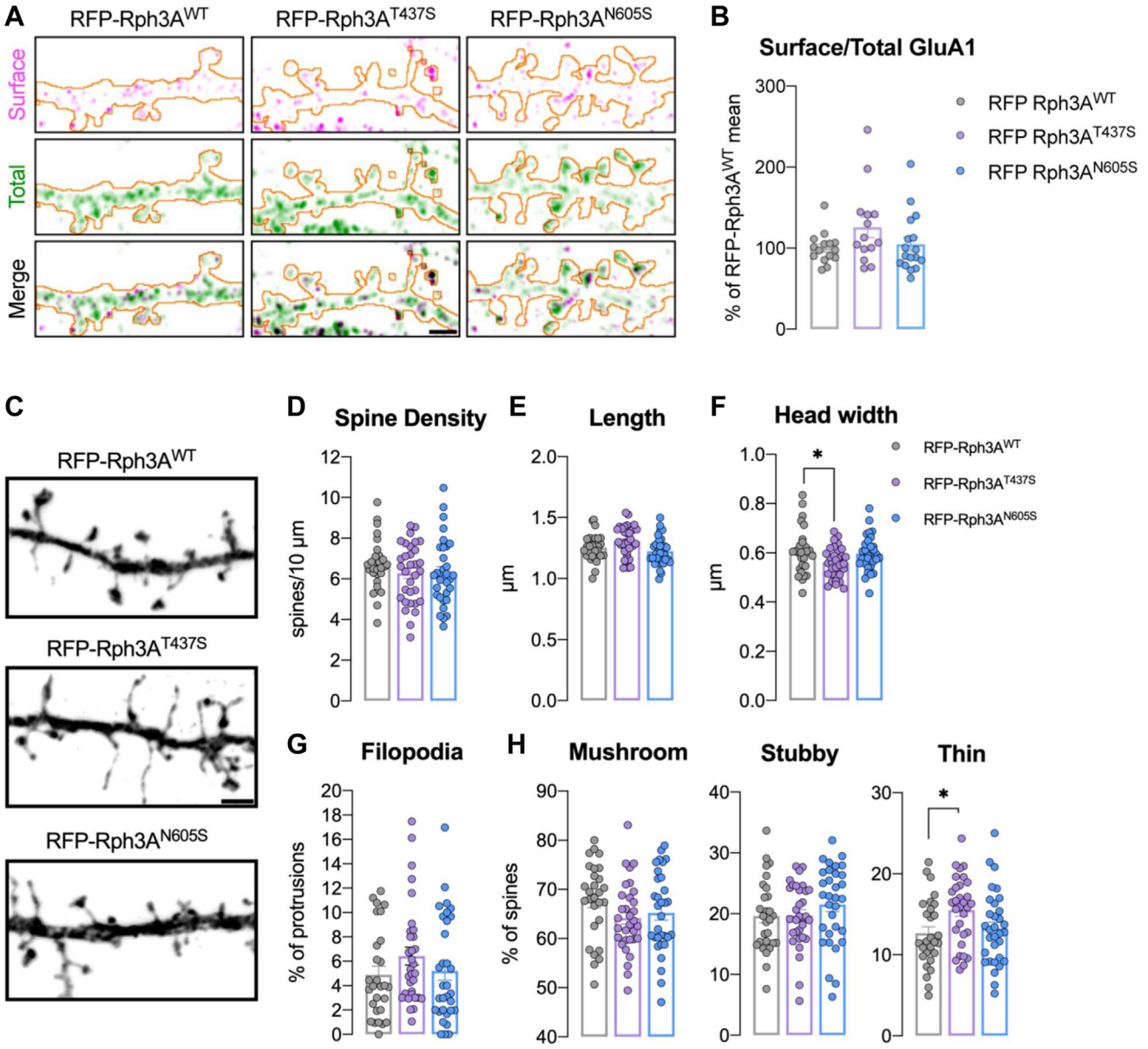

Figure 5 Evaluation of surface GluA1, spine density, and morphology. A. Confocal images of surface (magenta) and total GluA1 (green) staining of RFP-Rph3A^{WT}, RFP-Rph3A^{N605S}, or RFP-Rph3A^{T437S} transfected neurons (orange outline). Scale bar: 2 µm. B. A bar graph representing the mean ± SEM of the percentage of RFP-Rph3A^{WT} GluA1 surface/total ratio, Kruskal-Wallis test with Dunn's post hoc test was used. Dots represent single values. C. Confocal images of GFP filler in the dendritic spines of RFP-Rph3A^{WT}, RFP-Rph3A^{N605S}, or RFP-Rph3A^{T437S} transfected neurons were taken. The scale bar is 2 µm. B-F. Bar graph representation of the mean ± SEM spine density (D), spine length (E), spine head width (F), filopodia proportions (G), and spine types percentage (H) in RFP-Rph3A^{WT}, RFP-Rph3A^{N605S}, or RFP-Rph3A^{T437S}-transfected neurons were also taken. An ordinary one-way ANOVA with Dunnett's post hoc test (spine density, length, head width, mushroom, or stubby), and a Kruskal-Wallis test with Dunn's post hoc test (filopodia, thin) were used. *$P < .05$. Dots represent single values. ANOVA, analysis of variance; SEM, scanning electron microscopy.

and an ultra-rare NDD with variable expressivity. This disorder is associated with epilepsy, ID, or ASD and learning disability.

Data Availability

The data supporting the findings of this study are available from the corresponding author.

Acknowledgments

The authors are grateful to patients and their families for their participation in this study.

Funding

This research received funding from the Italian Ministry for Education, University and Research (Ministero

dell'Istruzione, dell'Università e della Ricerca - MIUR) PRIN2020 code 20203P8C3X to A.B., PRIN2017 code 2017ENN4FY to F.G., "Associazione E.E. Rulfo per la genetica Medica" to A.B., and Fondazione Cassa di Risparmio di Torino to A.B. and M.G. Sample collection was supported by the NIMH (U01MH111661 to J.D.B.).

This work was supported by a grant from the US National Human Genome Research Institute (NHGRI; UM1HG007301) to S.M.H. This study was funded by the MRC (MR/S01165X/1, MR/S005021/1, G0601943, MR/V012177/1), The National Institute for Health Research University College London Hospitals Biomedical Research Centre, Rosetree Trust, Ataxia UK, MSA Trust, Brain Research UK, Sparks GOSH Charity, Muscular Dystrophy UK (MDUK), and Muscular Dystrophy Association (MDA USA).

This research was made possible through access to the data and findings generated by the 100,000 Genomes Project. The 100,000 Genomes Project is managed by Genomics England Limited (a wholly owned company of the Department of Health and Social Care). The 100,000 Genomes Project is funded by the National Institute for Health Research and NHS England. The Wellcome Trust, Cancer Research UK and the Medical Research Council have also funded research infrastructure. The 100,000 Genomes Project uses data provided by patients and collected by the National Health Service as part of their care and support.

Author Information

Conceptualization: L.Pav., J.S., F.G., M.G., A.B.; Data Curation: L.Pav., J.S., M.B., A.G., V.C.; Investigation: L.Pav., J.S., M.B., A.G., G.C., V.C., I.E., L.P, M.D.L., A.C., A.M., E.B., M.S., S.M.H., W.V.K., L.V., S.M.S., S.E., P.C., R.K., A.B., S.C., M.T., S.D.R., J.D.B., D.S.; Supervision: M.G., F.G., A.B.; Writing-original draft: L.Pav., J.S., M.G., F.G., A.B.; Writing-review and editing: L.Pav., J.S., A.G., A.M., I.E., V.C., G.B.F., M.G., F.G., A.B.

Ethics Declaration

Informed consent was obtained from participating families, and the study protocol was approved by the Internal Ethics Committee of the University of Turin (n. 0060884), in accordance to the Declaration of Helsinki. Part of the cases were collected within the 100,000 Genomes Project and had specific ethical approval.

Conflict of Interest

The authors declare no conflicts of interest.

Additional Information

The online version of this article (https://doi.org/10.1016/j.gim.2023.100922) contains supplemental material, which is available to authorized users.

Web Resources

GnomAD, https://gnomad.broadinstitute.org/
InterPro, http://www.ebi.ac.uk/interpro/

Authors

Lisa Pavinato[1,2,3], Jennifer Stanic[4], Marta Barzasi[4], Antonia Gurgone[5], Giuseppe Chiantia[5], Valentina Cipriani[6], Ivano Eberini[4], Luca Palazzolo[4], Monica Di Luca[4], Alex Costa[7,8], Andrea Marcantoni[9], Elisa Biamino[10], Marco Spada[10], Susan M. Hiatt[11], Whitley V. Kelley[11], Letizia Vestito[6], Sanjay M. Sisodiya[12,13], Genomics England Research Consortium, Stephanie Efthymiou[14], Prem Chand[15], Rauan Kaiyrzhanov[16], Alessandro Bruselles[17], Simona Cardaropoli[18], Marco Tartaglia[19], Silvia De Rubeis[20,21,22,23], Joseph D. Buxbaum[20,21,22,23,24], Damian Smedley[6], Giovanni Battista Ferrero[25], Maurizio Giustetto[5], Fabrizio Gardoni[4], Alfredo Brusco[1,26,*]

Affiliations

[1]Department of Medical Sciences, University of Turin, Turin, Italy; [2]Institute of Oncology Research (IOR), Bellinzona, Switzerland; [3]Università della Svizzera Italiana, Lugano, Switzerland; [4]Department of Pharmacological and Biomolecular Sciences, DiSFeB, University of the Studies of Milan, Milan, Italy; [5]Department of Neuroscience, University of Turin, Turin, Italy; [6]William Harvey Research Institute, Clinical Pharmacology Precision Medicine, Queen Mary University of London, Charterhouse Square, United Kingdom; [7]Department of Biosciences, University of the Studies of Milan, Milan, Italy; [8]Institute of Biophysics, Consiglio Nazionale delle Ricerche (CNR), Milan, Italy; [9]Department of Drug Science and Technology, University of Turin, Turin, Italy; [10]Department of Pediatrics, Regina Margherita Children Hospital, Turin, Italy; [11]HudsonAlpha Institute for Biotechnology, Huntsville, AL; [12]Department of Clinical and Experimental Epilepsy, UCL Queen Square Institute of Neurology, London, United Kingdom; [13]Chalfont Centre for Epilepsy Bucks, Chalfont St Peter, United Kingdom; [14]Department of Neuromuscular Diseases, UCL Queen Square Institute of Neurology, London, United Kingdom; [15]Department of Paediatric and Child Health, Aga Khan University Hospital, Karachi, Pakistan; [16]University College London, UCL Queen Square Institute of

Neurology, London, United Kingdom; [17]Department of Oncology and Molecular Medicine, Istituto Superiore di Sanità, Rome, Italy; [18]Department of Public Health and Pediatric Sciences, University of Torino, Torino, Italy; [19]Genetics and Rare Diseases Research Division, Ospedale Pediatrico Bambino Gesù, IRCCS, Rome, Italy; [20]Seaver Autism Center for Research and Treatment, Icahn School of Medicine at Mount Sinai, New York, NY; [21]Department of Psychiatry, Icahn School of Medicine at Mount Sinai, New York, NY; [22]The Mindich Child Health and Development Institute, Icahn School of Medicine at Mount Sinai, New York, NY; [23]Friedman Brain Institute, Icahn School of Medicine at Mount Sinai, New York, NY; [24]Department of Neuroscience, Icahn School of Medicine at Mount Sinai, New York, NY; [25]Department of Clinical and Biological Sciences, University of Turin, Orbassano, TO, Italy; [26]Medical Genetics Unit, Città della Salute e della Scienza University Hospital, Turin, Italy

References

1. Paoletti P, Bellone C, Zhou Q. NMDA receptor subunit diversity: impact on receptor properties, synaptic plasticity and disease. *Nat Rev Neurosci*. 2013;14(6):383-400. http://doi.org/10.1038/nrn3504
2. Bellone C, Nicoll RA. Rapid bidirectional switching of synaptic NMDA receptors. *Neuron*. 2007;55(5):779-785. http://doi.org/10.1016/j.neuron.2007.07.035
3. XiangWei W, Jiang Y, Yuan H. De novo mutations and rare variants occurring in NMDA receptors. *Curr Opin Physiol*. 2018;2:27-35. http://doi.org/10.1016/j.cophys.2017.12.013
4. Santos-Gómez A, Miguez-Cabello F, García-Recio A, et al. Disease-associated GRIN protein truncating variants trigger NMDA receptor loss-of-function. *Hum Mol Genet*. 2021;29(24):3859-3871. http://doi.org/10.1093/hmg/ddaa220
5. Fu JM, Satterstrom FK, Peng M, et al. Rare coding variation provides insight into the genetic architecture and phenotypic context of autism. *Nat Genet*. 2022;54(9):1320-1331. http://doi.org/10.1038/s41588-022-01104-0
6. de Rubeis S, He X, Goldberg AP, et al. Synaptic, transcriptional and chromatin genes disrupted in autism. *Nature*. 2014;515(7526):209-215. http://doi.org/10.1038/nature13772
7. Iossifov I, O'Roak BJ, Sanders SJ, et al. The contribution of de novo coding mutations to autism spectrum disorder. *Nature*. 2014;515(7526):216-221. http://doi.org/10.1038/nature13908
8. Endele S, Rosenberger G, Geider K, et al. Mutations in GRIN2A and GRIN2B encoding regulatory subunits of NMDA receptors cause variable neurodevelopmental phenotypes. *Nat Genet*. 2010;42(11):1021-1026. http://doi.org/10.1038/ng.677
9. Carvill GL, Regan BM, Yendle SC, et al. GRIN2A mutations cause epilepsy-aphasia spectrum disorders. *Nat Genet*. 2013;45(9):1073-1076. http://doi.org/10.1038/ng.2727
10. Strehlow V, Heyne HO, Vlaskamp DRM, et al. *GRIN2A* -related disorders: genotype and functional consequence predict phenotype. *Brain*. 2019;142(1):80-92. http://doi.org/10.1093/brain/awy304
11. Liu XR, Xu XX, Lin SM, et al. GRIN2A variants associated with idiopathic generalized epilepsies. *Front Mol Neurosci*. 2021;14:720984. http://doi.org/10.3389/fnmol.2021.720984
12. Lemke JR, Lal D, Reinthaler EM, et al. Mutations in GRIN2A cause idiopathic focal epilepsy with rolandic spikes. *Nat Genet*. 2013;45(9):1067-1072. http://doi.org/10.1038/ng.2728
13. Lesca G, Rudolf G, Bruneau N, et al. GRIN2A mutations in acquired epileptic aphasia and related childhood focal epilepsies and encephalopathies with speech and language dysfunction. *Nat Genet*. 2013;45(9):1061-1066. http://doi.org/10.1038/ng.2726
14. Elmasri M, Hunter DW, Winchester G, et al. Common synaptic phenotypes arising from diverse mutations in the human NMDA receptor subunit GluN2A. *Commun Biol*. 2022;5(1):174. http://doi.org/10.1038/s42003-022-03115-3
15. Bading H. Nuclear calcium signalling in the regulation of brain function. *Nat Rev Neurosci*. 2013;14(9):593-608. http://doi.org/10.1038/nrn3531
16. Franchini L, Stanic J, Ponzoni L, et al. Linking NMDA receptor synaptic retention to synaptic plasticity and cognition. *iScience*. 2019;19:927-939. http://doi.org/10.1016/j.isci.2019.08.036
17. Rodríguez-Palmero A, Boerrigter MM, Gómez-Andrés D, et al. DLG4-related synaptopathy: a new rare brain disorder. *Genet Med*. 2021;23(5):888-899. http://doi.org/10.1038/s41436-020-01075-9
18. Lelieveld SH, Reijnders MRF, Pfundt R, et al. Meta-analysis of 2,104 trios provides support for 10 new genes for intellectual disability. *Nat Neurosci*. 2016;19(9):1194-1196. http://doi.org/10.1038/nn.4352
19. Stanic J, Carta M, Eberini I, et al. Rabphilin 3A retains NMDA receptors at synaptic sites through interaction with GluN2A/PSD-95 complex. *Nat Commun*. 2015;6:10181. http://doi.org/10.1038/ncomms10181
20. Franchini L, Stanic J, Barzasi M, et al. Rabphilin-3A drives structural modifications of dendritic spines induced by long-term potentiation. *Cells*. 2022;11(10):1616. http://doi.org/10.3390/cells11101616
21. Satterstrom FK, Kosmicki JA, Wang J, et al. Large-scale exome sequencing study implicates both developmental and functional changes in the neurobiology of autism. *Cell*. 2020;180(3):568-584.e23. http://doi.org/10.1016/j.cell.2019.12.036
22. Karczewski KJ, Francioli LC, Tiao G, et al. The mutational constraint spectrum quantified from variation in 141,456 humans. *Nature*. 2020;581(7809):434-443. http://doi.org/10.1038/s41586-020-2308-7
23. Sobreira N, Schiettecatte F, Valle D, Hamosh A. GeneMatcher: a matching tool for connecting investigators with an interest in the same gene. *Hum Mutat*. 2015;36(10):928-930. http://doi.org/10.1002/humu.22844
24. Caulfield M, Davies J, Dennys M, Elbahy L, Fowler T, Hill S. The National Genomics Research and Healthcare Knowledgebase Amendment to the 100,000 Genomes Project Protocol v4. 2017. https://doi.org/10.6084/m9.figshare.4530893.v5
25. Samocha KE, Robinson EB, Sanders SJ, et al. A framework for the interpretation of de novo mutation in human disease. *Nat Genet*. 2014;46(9):944-950. http://doi.org/10.1038/ng.3050
26. Gaildrat P, Killian A, Martins A, Tournier I, Frébourg T, Tosi M. Use of splicing reporter minigene assay to evaluate the effect on splicing of unclassified genetic variants. *Methods Mol Biol*. 2010;653:249-257. http://doi.org/10.1007/978-1-60761-759-4_15
27. Montaville P, Schlicker C, Leonov A, Zweckstetter M, Sheldrick GM, Becker S. The C2A-C2B linker defines the high affinity Ca(2+) binding mode of rabphilin-3A. *J Biol Chem*. 2007;282(7):5015-5025. http://doi.org/10.1074/jbc.M606746200
28. Guillén J, Ferrer-Orta C, Buxaderas M, et al. Structural insights into the Ca^{2+} and $PI(4,5)P_2$ binding modes of the C2 domains of rabphilin 3A and synaptotagmin 1. *Proc Natl Acad Sci U S A*. 2013;110(51):20503-20508. http://doi.org/10.1073/pnas.1316179110
29. Coudevylle N, Montaville P, Leonov A, Zweckstetter M, Becker S. Structural determinants for Ca2+ and phosphatidylinositol 4,5-bisphosphate binding by the C2A domain of Rabphilin-3A. *J Biol Chem*. 2008;283(51):35918-35928. http://doi.org/10.1074/jbc.M804094200
30. Gurgone A, Pizzo R, Raspanti A, et al. mGluR5 PAMs rescue cortical and behavioural defects in a mouse model of CDKL5 deficiency disorder. *Neuropsychopharmacology*. 2023;48(6):877-886. http://doi.org/10.1038/s41386-022-01412-3
31. Marcantoni A, Cerullo MS, Buxeda P, et al. Amyloid Beta42 oligomers up-regulate the excitatory synapses by potentiating presynaptic release while impairing postsynaptic NMDA receptors. *J Physiol*. 2020;598(11):2183-2197. http://doi.org/10.1113/JP279345

32. Hardingham GE, Bading H. Synaptic versus extrasynaptic NMDA receptor signalling: implications for neurodegenerative disorders. *Nat Rev Neurosci*. 2010;11(10):682-696. http://doi.org/10.1038/nrn2911
33. Brozzi F, Diraison F, Lajus S, et al. Molecular mechanism of myosin Va recruitment to dense core secretory granules. *Traffic*. 2012;13(1):54-69. http://doi.org/10.1111/j.1600-0854.2011.01301.x
34. Correia SS, Bassani S, Brown TC, et al. Motor protein–dependent transport of AMPA receptors into spines during long-term potentiation. *Nat Neurosci*. 2008;11(4):457-466. http://doi.org/10.1038/nn2063
35. Maselli RA, Vázquez J, Schrumpf L, et al. Presynaptic congenital myasthenic syndrome with altered synaptic vesicle homeostasis linked to compound heterozygous sequence variants in *RPH3A*. *Mol Genet Genomic Med*. 2018;6(3):434-440. http://doi.org/10.1002/mgg3.370
36. Suzuki T, Koike Y, Ashikawa K, et al. Genome-wide association study of epilepsy in a Japanese population identified an associated region at chromosome 12q24. *Epilepsia*. 2021;62(6):1391-1400. http://doi.org/10.1111/epi.16911
37. Stanic J, Mellone M, Napolitano F, et al. Rabphilin 3A: a novel target for the treatment of levodopa-induced dyskinesias. *Neurobiol Dis*. 2017;108:54-64. http://doi.org/10.1016/j.nbd.2017.08.001
38. Schlüter OM, Schnell E, Verhage M, et al. Rabphilin knock-out mice reveal that rabphilin is not required for Rab3 function in regulating neurotransmitter release. *J Neurosci*. 1999;19(14):5834-5846. http://doi.org/10.1523/JNEUROSCI.19-14-05834.1999